Antiproton annihilation at rest in nitrogen and deuterium gas

J. Riedlberger, C. Amsler, M. Doser,[a] U. Straumann, and P. Truöl
Physik Institut der Universität Zürich, 8001 Zürich, Switzerland

D. Bailey,[b] S. Barlag,[c] U. Gastaldi, R. Landua, and C. Sabev
Counseil Européen pour la Recherche Nucleaire, 1211 Genève, Switzerland

K. D. Duch,[d] M. Heel,[e] H. Kalinowsky, F. Kayser,[f] E. Klempt, B. May,
O. Schreiber,[g] P. Weidenauer, and M. Ziegler[h]
Institut für Physik, Johannes-Gutenberg-Universität, 6500 Mainz, Germany

W. Dahme,[i] F. Feld-Dahme,[j] U. Schaefer,[k] and W. R. Wodrich[d]
Sektion Physik, Ludwig-Maximilians-Universität, 8000 München, Germany

S. Ahmad,[l] J. C. Bizot, B. Delcourt, J. Jeanjean, H. Nguyen, and N. Prevot[m]
Laboratoire de l'Accélérateur Linéaire, Université de Paris-Sud, 91405 Orsay, France

E. G. Auld, D. A. Axen, K. L. Erdman, B. Howard, R. Howard, and B. L. White
Department of Physics, University of British Columbia, Vancouver, British Columbia, Canada V6T 2A6

M. Comyn
TRIUMF, Vancouver, British Columbia, Canada V6T 2A3

G. Beer, G. M. Marshall,[l] and L. P. Robertson
Department of Physics, University of Victoria, Victoria, British Columbia, Canada V8W 2Y2

M. Botlo,[n] C. Laa,[o] and H. Vonach
Institut für Kernphysik, Universität Wien, 1090 Wien, Austria
(Received 22 May 1989)

Results on antiproton absorption at rest in gaseous nitrogen and deuterium are presented from an analysis of approximately 10^6 events each taken with a magnetic spectrometer. Inclusive features such as pion and proton multiplicities and spectra are presented. Data relating to absorption modes requiring more than one nucleon, such as the Λ yield, the Λ spectrum, and the exclusive deuterium channels $\bar{p}d \rightarrow \pi^- p$, $\Lambda K^+ \pi^-$ are discussed. The fully reconstructable channels $\bar{p}d \rightarrow \pi^+ \pi^- \pi^- p, \pi^+ \pi^+ \pi^- \pi^- \pi^- p$ also show a high-energy proton tail unaccounted for by single nucleon rescattering mechanisms.

I. INTRODUCTION

The ASTERIX spectrometer[1] (antiproton stop experiment with trigger on initial x rays) was operated at the low-energy antiproton ring (LEAR) at CERN to study $\bar{p}p$ annihilation at rest in hydrogen gas. The ongoing analysis of the several million events focuses on meson spectroscopy,[2,3] while the published data have dealt with protonium x rays[4] and two-body annihilation channels.[5] In this paper we report on a smaller data sample with gaseous nitrogen (7×10^5 events) and deuterium (10^6 events) targets. Our interest in this deviation from the main goals of the experiment was stimulated by a pilot study of $\bar{p}$-annihilation events in argon,[6] which appeared as an unwanted background in our 1983 run, when the minimum antiproton momentum accessible at LEAR was 300 MeV/c and the $\bar{p}$-stopping distribution showed tails extending into the argon circulating through our innermost drift chamber. This study made us realize that,

apart from early bubble-chamber[7−11] and emulsion[12] data of limited statistical significance, nearly no data exist for nuclear antiproton absorption at rest into exclusive channels and that even the single-particle inclusive spectra for pions and nucleons are known for but a few nuclei.[13] The experimental situation is slightly more favorable for annihilation in flight at 600 MeV/c, where LEAR experiments have furnished data on pion, proton, and other charged particle multiplicities and spectra for ^{20}Ne (Ref. 14), ^{12}C, ^{89}Y, and ^{238}U (Ref. 15).

The shortage of data on nuclear antiproton absorption is particularly noticeable if a serious attempt is being made to test an increasing number of theoretical calculations dealing with this subject. Extensive predictions exist from three variants of an intranuclear cascade model originating from Moscow,[16,17] Liège (Belgium),[18,19] and Los Alamos.[20] The basic philosophy of these codes is similar and also in agreement with the main features of the nuclear annihilation process, which is pictured as a

quasifree annihilation on a bound nucleon at the nuclear surface and the subsequent interaction of the annihilation products with the remaining nucleus. The initial pion and kaon multiplicities and momentum distributions are modeled after the existing hydrogen and deuterium data. The observed distributions in the nuclear case, as our data also show, do not differ very much from the nucleon case. The pion multiplicity, at least for the lighter nuclei, decreases only by 5 to 10% and the seemingly thermal nature of the pion, proton, and lambda spectra reflects essentially the Maxwell-Boltzmann-type distribution of the corresponding proton and deuterium distributions, which are well described by a single temperature parameter.[13,21−23] However, it is also apparent that the examination of these global features will not suffice, if a more detailed understanding of how the multimeson final state propagates through the nuclear environment is to be achieved. The influence of pion absorption (on two nucleons) versus the scattering of the pions on single nucleons, the role of the Δ resonance, issues which traditionally have also been debated for pion-nucleus interactions, are also appearing here.[16,17,19,24,25] In this context the study of correlations between the particles in the final state may be particularly useful. Invariant mass distributions of pion-proton pairs may signal the Δ resonance[19] and two-nucleon invariant mass distributions, the pion absorption,[24] or even the more exotic absorption mechanisms of meson resonances such as η and ω, first advocated by Iljinov *et al.*[16] For this purpose a large solid angle spectrometer, as the ASTERIX detector was well suited, and our study may provide guidance for the more ambitious program of the OBELIX experiment[26] planned at LEAR. The direct comparison with the proton and deuterium data taken with the same detector eliminates to a large extent the experimental uncertainties in the nuclear to nucleon comparison, in particular those arising from the incomplete solid angle.

A certain class of antiproton reactions at rest is only possible with $A \geq 2$, since it involves the interaction of the $\bar{p}$ with at least two nucleons. It includes all channels with a hyperon in the final state, such as $\bar{p}N(A,Z) \rightarrow N(A-2,Z-1)\Lambda K(m\pi)$ and "Pontecor-

vo"[27] reactions like $\bar{p}d \rightarrow \pi^- p$. These reactions can occur via conventional mechanisms, normally described by triangular graphs (Fig. 1), where $\bar{p}p$ or $\bar{p}n$ annihilation on a bound nucleon (baryon number $B=0$) is followed by absorption or charge exchange of the primary pion (or kaon) on another nucleon. They can also occur as a direct $B=1$ process with—on the quark level—rearrangement, annihilation, or creation of $\bar{q}q$ pairs starting from a $(6q\,3\bar{q})$ system. Predictions exist within a statistical model[28] and a model where pions produced in the annihilation may be off the mass shell creating nuclear particle-hole pairs.[29] Already the first bubble-chamber study of $\bar{p}\,{}^{12}C$ contains one very nice example of a Λ event.[7] We have studied inclusive Λ production for ${}^{14}N$ and exclusive channels for ${}^2H$, for which limited previous data exist.[13,30] The inclusive strange-particle yield has also been mentioned in connection with speculations that the $\bar{p}$ annihilation may transfer enough energy to the nucleus[31] to create a new phase of nuclear matter, the quark gluon plasma phase.[32−34] These models were stimulated by the observation of a high yield of Λ's from $\bar{p}$ Ta interaction at 4 GeV/c (about 10% of the total cross section)[35] and a substantial high-energy tail in the spectator proton distribution in $\bar{p}d \rightarrow K\bar{K}(m\pi)p_s$.[36] For the channels $\bar{p}d \rightarrow 2\pi^- \pi^+ p_s$ and $\bar{p}d \rightarrow 3\pi^- 2\pi^+ p_s$ we have reconstructed the proton spectrum either from visible protons or from the pions only. The high-energy tail is observed, too, as has been shown previously with less statistics in bubble chambers,[21−23] i.e., associated strangeness production is by no means a prerequisite for this tail. However, a satisfactory explanation does not exist yet.[37] For complex nuclei the high-energy proton tail was also unaccounted for in early intranuclear cascade calculations.[20] It has, however, been argued[19] that enough uncertainty exists in these models for a conventional explanation of this feature. Off-shell pion production in $\bar{p}N$ may also enhance high-energy nucleon emission,[38] but again a description of the complete spectrum has not been achieved. Only more precise data on more nuclei will help to solve these problems.

The deuterium data also yielded, as a byproduct, branching ratios for the following channels:
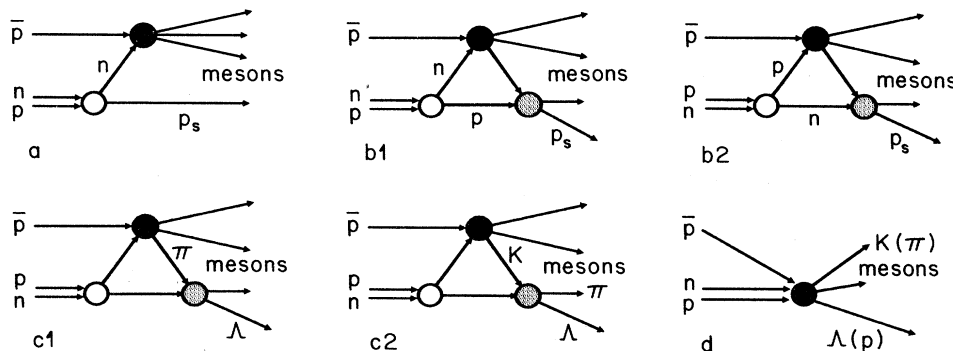
FIG. 1. Possible mechanisms for nuclear $\bar{p}$ absorption illustrated for deuterium. a: Annihilation on the neutron with a low momentum proton spectator. b1: Rescattering with a resulting high momentum proton. b2: Charge exchange. c1 (c2): Λ production by π (K) rescattering. d: Two-nucleon annihilation.
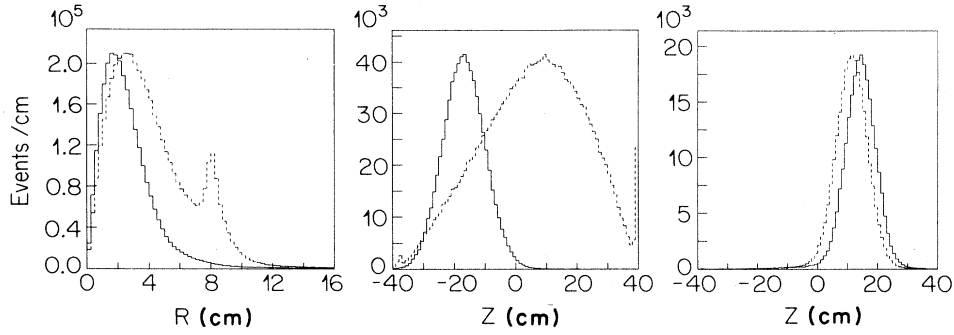
FIG. 2. Radial (left) and axial (center and right) distribution of annihilation vertices. Left and center: 200 MeV/c $\bar{p}$: solid curve: $^{14}N_2$; dashed curve: $^1H_2$. Right: 100 MeV/c $\bar{p}$; solid curve: $^2H_2$; dashed curve: $^1H_2$. The $^1H_2$ distributions are multiplied by an arbitrary factor.

$\bar{p}d \rightarrow \pi^- p, \pi^+ \pi^- n_s$, $K^+ K^- n_s$, which are reported below. Lastly we have also used Bose-Einstein correlations of identical pions to study the space-time evolution of the pion source in $\bar{p}d$ and $\bar{p}$ ^{14}N (compared to $\bar{p}p$). These results, reported elsewhere[6,39] in general support the conclusion of a peripheral annihilation with only mild influence on the nucleus.

II. EXPERIMENTAL DETAILS

A. Setup

For our nitrogen data antiprotons were extracted from LEAR with a momentum of 200 MeV/c. After passing through suitable degraders and a beam defining scintillator they entered a gas target (length 80 cm) with a residu-

al momentum of 68 MeV/c and then stopped near the center of the target. The range straggling produced a Gaussian annihilation depth of 20 mg/cm^2 full width (see Fig. 2). At this momentum the hydrogen stopping distribution was three times wider in length and also extended radially into the drift chamber, which surrounded the target. To avoid acceptance corrections we prefer to compare our nitrogen data to the deuterium and hydrogen data taken one year later with 100 MeV/c $\bar{p}$ momentum, which showed similar radial and axial distribution of annihilation vertices. The average antiproton intensity used was $3 \times 10^4 \bar{p}$ sec^{-1}.

For completeness we show our spectrometer in Fig. 3, but limit its discussion to those features relevant to the data presented here. The drift chamber (XDC) was equipped with a 6 μm Mylar inner window transparent to
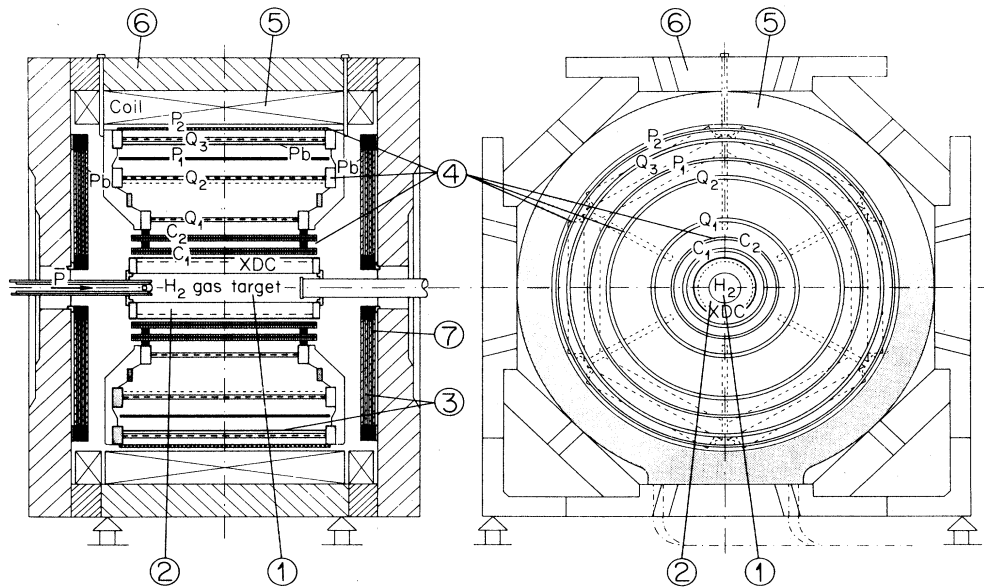
FIG. 3. The ASTERIX spectrometer. (1) Hydrogen (nitrogen) gas target. The small disks at the end and at the entrance are the scintillators defining the incoming $\bar{p}$ and vetoing a nonstopping $\bar{p}$, respectively. (2) Spiral projection chamber (50% Ar, 50% C_2H_6 gas). (3) Lead foils to convert photons. (4) Cylindrical multiwire proportional chambers; C_1, C_2, Q_1, Q_2, Q_3 with anode (wires parallel to beam axis) and cathode readout (helical strips); P_1, P_2 anode readout only. (5) Coils and (6) yoke to produce a 0.8 Tesla axial field. (7) Endcaps with hexagonal multiwire proportional chambers for position-sensitive photon detection.
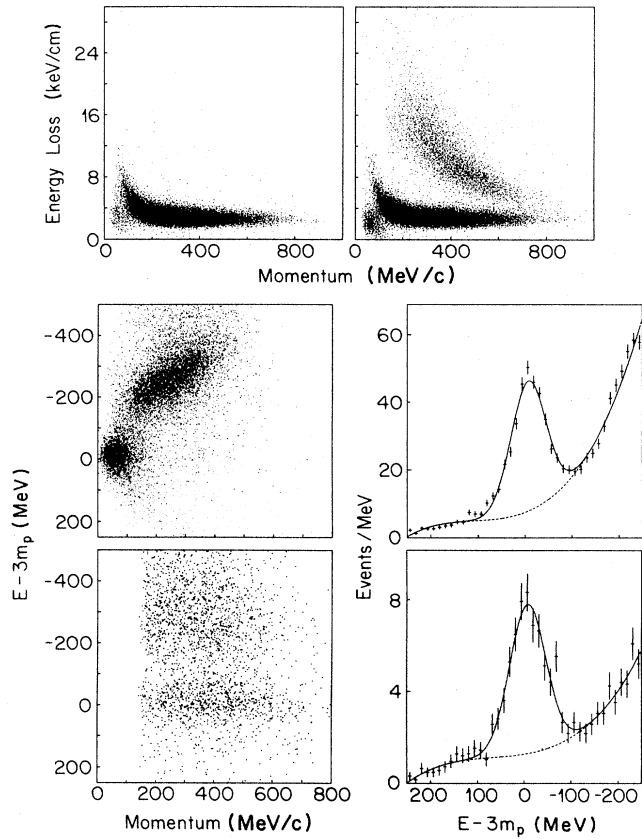
FIG. 4. Top: Truncated mean of pulseheight in the XDC (N_2). Left: Negative particles; right: positive particles. Center and bottom (left): $\bar{p}d \rightarrow 3\pi^- 2\pi^+ m\pi^0 p_s$ scatterplot total energy ($-3m_p$) versus total momentum ($|\mathbf{p}|$) of the pions with no proton seen (center) in the five-prongs data sample and versus the proton momentum (bottom) in the six-prongs data sample with one detected proton. Right: Projections onto the energy axis. The dashed line indicates the polynomial fit to the background under the peak.

gy loss per path length. We used this information to discriminate protons against pions. The truncated mean energy loss versus momentum of the particles is shown in Fig. 4 for positive and negative particles; the proton band is clearly visible. Kaons could in principle be distinguished too,[1] but in the nuclear case they disappear in the tails of the pion and proton distributions, which are somewhat wider than reached in other runs,[1] because during the N_2 runs less calibration data were taken. The energy-loss distribution for positive particles shows no peak indicating the clear presence of deuterons or heavier particles. Comparison of the deuterium target data with the nitrogen target furthermore show that these heavier particles could contribute at most 10% background to the proton spectrum; below 300 MeV/c deuterons cannot be observed due to insufficient range. These findings are consistent with the ^{12}C results of Ref. 13 which give a deuteron to proton rate of 9%. With the seven cylindrical multiwire proportional chambers ($C_1, C_2, Q_1, Q_2, P_1, Q_3, P_2$) surrounding the XDC the pion momentum could be determined in the 0.8 T magnetic field with a typical resolution of 7.5% full width at half maximum (FWHM) (deduced from exclusive channels in H_2, Ref. 1), while the proton momentum could only be measured to 15% due to multiple scattering (estimated from the width of Λ signal, see below). Our complete data sample comprises 3.4×10^5 events for N_2 and 1.3×10^5 events for D_2 taken with the minimum bias $\bar{p}$-stop trigger condition, requiring only the disappearance of an antiproton in the target. 3.3×10^5 and 4.0×10^5 events, respectively, were taken with a multiwire proportional chamber (MWPC) multiplicity trigger,[1] which required at least two hits in chambers C_1, C_2, Q_2, and P_1. For $^2H_2$ an additional sample of high multiplicity ($\geq$ four tracks) sample of 5×10^5 events was taken, too. All inclusive spectra and particle multiplicities are derived from the minimum bias data. The information from the γ detectors mounted on the endcaps of the solenoid was ignored in our analysis.

B. Pion and proton spectra

After pion and proton separation the projection of the two-dimensional spectra shown in Fig. 4 onto the momentum axis is displayed in Figs. 5 and 6. For pions (Fig. 5) the acceptance of our spectrometer reached a plateau of 70% (see next chapter) for $p_\pi > 80$ MeV/c; the minimum detectable momentum was 40 MeV/c. At these low momenta pattern recognition was found to be

low-energy x rays. We observed the higher principal quantum number lines of the antiprotonic nitrogen atom cascade ($n = 10$ to $n = 6$, see Ref. 6), but not those immediately preceding the absorption from the $n = 3$ level, since the XDC, which was designed for the detection of the Lyman and Balmer series in protonium,[4] was not efficient for the 56 keV, $n = 4$ to $n = 3$ transition.[40] However, the integrated charge collected on several sense wires in the XDC also gave multiple samples of the ener-

FIG. 5. Pion momentum spectra for ^1H, ^2H, and ^{14}N. The curves show the Maxwell-Boltzmann distribution fits to the spectrum (see text for limits). For hydrogen and deuterium the low-energy part is not in agreement with this ansatz (see also Fig. 7).
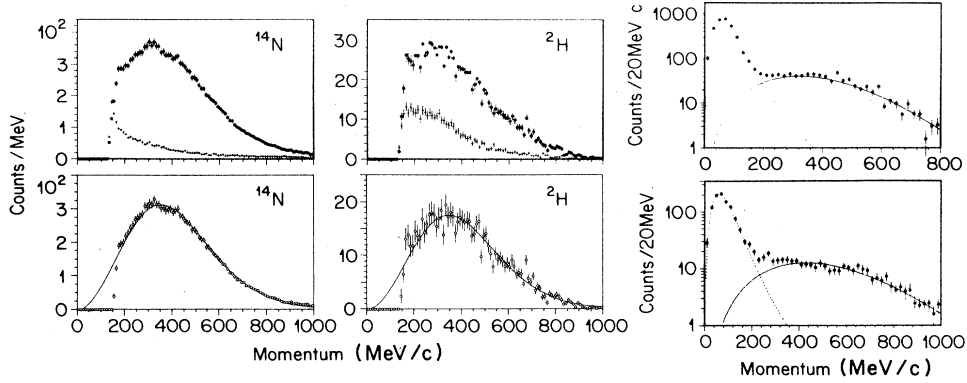
FIG. 6. Left and center: inclusive proton spectra for nitrogen and deuterium; top: proton candidates and pion contamination extrapolated from fitting the π^- spectrum to the proton spectrum in a selected subregion of the energy loss; bottom: background subtracted spectra. Right: complete proton spectra for $\bar{p}d \rightarrow 3\pi^- 2\pi^+ p_s$ (top) and $\bar{p}d \rightarrow 2\pi^- \pi^+ p_s$ (bottom); dotted curve: Fourier transform of Hulthén wave function; solid curve: Maxwell-Boltzmann distribution.

unreliable, because normally only four track points were seen. Thus we exclude the region below 80 MeV/c from all our considerations and also do not attempt to interpret possible structures seen there. The probability for pion decay before chamber Q_1 was less than 5% for $p_\pi > 150$ MeV/c. For a relativistic Maxwell-Boltzmann distribution the momentum spectrum follows

$$dN/dp = A\,(p^2/E)\exp(-E/E_0)\,,$$

where the normalization constant A and the temperature E_0 are experimental parameters. For hydrogen and deuterium such a parametrization only describes the pion spectra above $p_\pi > 300$ MeV/c, whereas in N_2 the lower limit is 100 MeV/c (Fig. 7). Table I lists the parameters.

The proton spectra require two adjustments. First, at least 130 MeV/c of transverse momentum is required to reach P_1. This includes the energy loss in the XDC outer

shell and in the MWPC's (270 mg/cm^2) and explains the sharp low momentum cutoff in the proton spectrum. We determined the proton momenta from the track sections between chambers C_1 and P_1 and corrected for the energy loss before C_1 by tracking the protons back to the target. Secondly, the spectrum of proton candidates (Fig. 6) had to be corrected for the pion contamination (see Figs. 4 and 6). The background free spectra can also be fitted with a Maxwell-Boltzmann ansatz and the temperatures are listed in Table I.

For two exclusive channels in deuterium the reconstruction of the complete proton spectrum is possible, because all pions are charged and detected. Figure 4 shows the total energy carried by the five pions and by the proton ($E = \sum_{i=1}^5 E_{\pi i} + E_p - 3m_p$) versus the total pion momentum ($|\mathbf{p}_p| = |\sum_{i=1}^5 \mathbf{p}_i|$) or the measured proton momentum for the channel $\bar{p}d \rightarrow 2\pi^+ 3\pi^- (p_s)$. Since the spectator proton carries only momentum, but nearly no
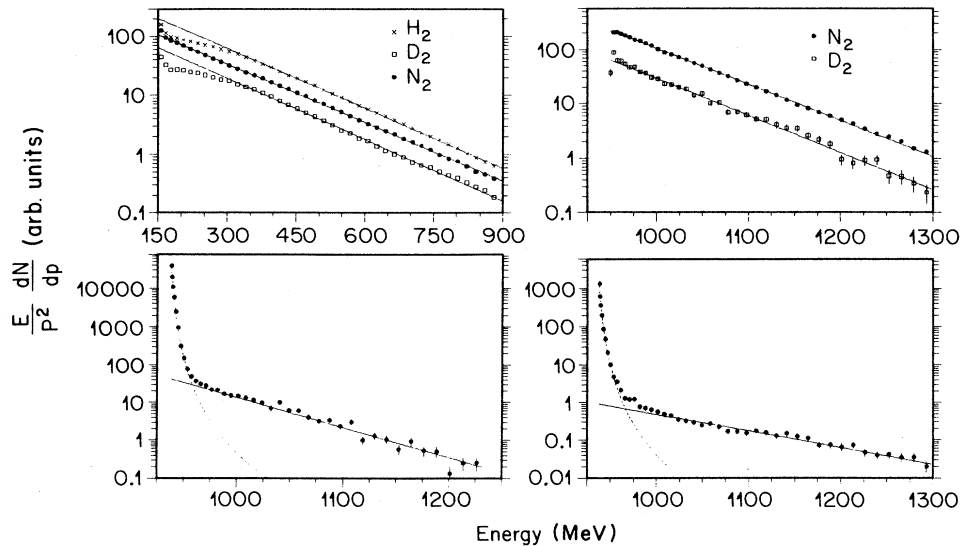
FIG. 7. Maxwell-Boltzmann fits to the momentum spectra: $E/p^2 * dN/dp \sim e^{-E/T}$. The temperatures are given in Table I. Top left: pions, top right: protons, bottom left: $\bar{p}d \rightarrow 3\pi^- 2\pi^+ p_s$, bottom right: $\bar{p}d \rightarrow 2\pi^- \pi^+ p_s$.

TABLE I. Parameters for the fits to the pion and proton spectra of Figs. 5 and 6. E_0: Temperature characteristic for the Maxwell-Boltzmann distribution; Y_s, Y_{MB} relative yields for the spectator and thermal part of the spectrum respectively; μ: Range parameter for the Hulthén wave function.

Target	Channel	Particle	Range of fit (GeV/c)	Parameter	Results This experiment	Other experiments
^{1}H	all	$\pi^\pm$	$0.3 \le p_\pi \le 0.9$	E_0 (MeV)	128±1	128±1, Ref. 21
^{2}H		π^-	$0.3 \le p_\pi \le 0.9$	E_0 (MeV)	126±1	124±1, Ref. 21
^{14}N		π^-	$0.1 \le p_\pi \le 0.9$	E_0 (MeV)	131±1	
^{12}C		π^-		E_0 (MeV)		136±3, Ref. 13
^{2}H	all	p	$0.2 \le p_p \le 0.9$	E_0 (MeV)	64±1	
^{14}N		p	$0.2 \le p_p \le 0.9$	E_0 (MeV)	66±1	
^{12}C		p		E_0 (MeV)		78±4 Ref. 13
^{2}H	$3\pi^- 2\pi^+$	p	$p_p \le 0.2$	Y_s (%)	79±2	
				μ (MeV/c)	87±2	
			$P_p \ge 0.2$	Y_{MB} (%)	21±2	23±1, Ref. 54
				E_0 (MeV)	55±1	
^{2}H	$2\pi^- \pi^+$	p	$p_p \le 0.2$	Y_s (%)	75±2	
				μ (MeV/c)	105±2	
			$p_p \ge 0.2$	Y_{MB} (%)	25±2	25±2, Ref. 22
				E_0 (MeV)	98±3	80, Ref. 22

kinetic energy, the events without any missing π^0 production cluster along the $E=0$ line, for higher momentum the proton is actually seen in most cases. Projecting slices in momentum onto the energy axis and fitting a third-order polynomial to the π^0 background, as indicated in Fig. 4, yields the background free spectra shown in Figs. 6 and 7. The $\bar{p}d \to \pi^+ 2\pi^- (p_s)$ channel is treated similarly. The spectra can be fitted with the Fourier transform of an exponential Hulthén wave function $\{f(p) \sim [(p/\mu^2 + p^2)]^2\}$ and a Maxwell-Boltzmann distribution. Other features of the $\bar{p}d \to 2\pi^+ 3\pi^- (p_s)$ data related to the possible existence of broad mesons states[41] have been presented elsewhere.[42]

C. Meson multiplicities

Our detectors covered between 89% (innermost wire chamber) and 52% (outermost wire chamber) of the solid angle seen from the center of the detector. The effective threshold (corresponding to the point where 50% of the average efficiency is reached) for pions is 80 MeV/c, for protons 170 MeV/c. With the open cylinder geometry two tracks are less likely to be observed, if they are perpendicular. We recall these facts to indicate why the measurement of multiplicities could not reach the absolute accuracy of bubble-chamber experiments. However, the relative trends in the multiplicities for different targets could be determined quite well. The true multiplicities of charged mesons ($m_{ab}, a =$ number of $\pi^+, b =$ number of π^-) are obtained from the multiplicities of the observed tracks (n_{ab}) through a linear transformation: $n_{ab} = \sum_{ij} X_{abij} m_{ij}$. The transformation matrix X is the product of two matrices A and B, where B contains binomial coefficients multiplied with powers of the mean acceptance parameter q.

$$B_{abrs} = \begin{cases} 1 \text{ for } a = b = r = s = 0 \\ \begin{bmatrix} r \\ r-a \end{bmatrix} \begin{bmatrix} s \\ s-b \end{bmatrix} q^{(r+s)}(1-q)^{(r+s-a-b)} \text{ for } r \ge a, s \ge b \\ 0 \text{ otherwise .} \end{cases}$$

The second matrix A corrects for the empirical fact that, for high multiplicities, i.e., low average momenta and consequently short tracks, our pattern recognition program tends to mislabel a certain fraction of the tracks and furthermore even for low multiplicities and Monte Carlo generated tracks sometimes unphysical tracks are found, if the noise hits were mixed in with their observed frequencies.

$$A_{rsij} = \begin{cases} 1 - (r+s)\alpha \text{ for } r = i, s = j \\ \frac{1}{2}(r+s)\alpha \text{ for } r = i+1, s = j; r = i, s = j+1 \\ 0 \text{ otherwise .} \end{cases}$$

For $a + b \le 8$ (total observed pion multiplicity) and $|a - b| \le 3$ (net charge limited to $|Q| \le 3e$) the 27 experimental quantities are fitted with six parameters for hydrogen: the geometrical acceptance factor ($q = 0.725 \pm 0.008$), the probability that a track was unphysical ($\alpha = 0.038 \pm 0.006$), and the four true multiplicities m_{00}, m_{11}, m_{22}, and m_{33}. The inclusion of the parameter α changes the average multiplicity by approximately a factor $1 - \alpha$, but does not affect the distribution very much. It, however, significantly improves the fits to those components of the vector n_{ab} with large values of $|a \pm b|$. For deuterium the $m_{i,j+1}$ components (net

charge -1) also have to be included in the fit to account for annihilation on the neutron. Here the entries into the multiplicity distribution for positive tracks are weighted for π^+ and protons, according to their measured energy loss. Since we fix the acceptance (and α) at the hydrogen values we are left with eight free parameters. Since for nuclei secondary charge exchange processes like $\pi^+ n \to \pi^0 p$ or $\pi^- p \to \pi^0 n$ are possible, the net charge distribution is not limited to $Q=0$ or $-e$, but may extend, e.g., from $Q=2e$ to $Q=-3e$, if one allows up to two charge exchanges per event and does not include protons. For ^{14}N therefore the fit includes 22 parameters m_{ij}, with $|i-j| \le 3, i,j \le 4, i+j \le 7$. The results for the total pion multiplicities are summarized in Table II, while the net charge distributions are given in Table III. For hydrogen we find a slightly higher multiplicity than previously observed in bubble chamber. This could be due to the fact that we have used a gas target with 50% p-wave and 50% s-wave absorption, while in a bubble chamber s wave dominates. In deuterium the difference to previous values is small, for ^{14}N the multiplicities and net charge distributions are quite similar to the previously observed ones for ^{12}C.

The proton multiplicities listed in Table IV were obtained in a similar manner. In a first step the proton candidates ($|\mathbf{p}_p| \le 170$ MeV/c) are corrected for the pions surviving the dE/dx cut (33% in ^{2}H, 17% in ^{14}N). In a second step the geometrical acceptance is unfolded as described above, but including the fraction of protons lost by the dE/dx cut ($q_p = 0.51 \pm 0.04$ for ^{2}H and $q_p = 0.58 \pm 0.03$ for ^{14}N). We observe similar frequencies as previously seen in a propane bubble chamber for ^{12}C (Ref. 9, threshold not given, but typically 140 MeV/c can be deduced from other experiments[7]).

D. Lambda production

Figure 8 shows the invariant mass distribution of $p\pi^-$ pairs in the deuterium (top, left) and nitrogen (top, right) full data samples. The signal in the invariant-mass range [1112,1118] MeV/c^2 (90% confidence interval) contains 717 events in deuterium (664 events in nitrogen) superimposed on a background of 3665 (5585) events. This corresponds to 11 (8) standard deviations. The signal can be enhanced by requiring a long decay path for the Λ. When asking for the primary vertex to lie in the backward direction of the Λ momentum (see Fig. 8) the signal is reduced to 204 (198) events and the background to 182 (353) events. Figure 8 shows the spectrum for deuterium and nitrogen with this additional cut, the significance remains the same while the signal/background ratio is strongly enhanced. Since additional cuts can produce an unknown systematic bias, we use the original sample to calculate the Λ yield. For the deuterium sample we used only the $\bar{p}$-stop and two-prong data. In the four-prong trigger, channels like $\bar{p}d \to \Lambda K^0$; $K^0 = K_L$ or $K^0 \to 2\pi^0$ are suppressed. There is no such suppression of the signal in the two-prong data compared to the $\bar{p}$-stop data. However, the equivalent $\bar{p}$-stop number for the two-prong trigger needs to be determined for normalization. For this purpose we scale with the rate of all $p\pi^-$ combinations in the larger mass interval [1110,1120] MeV/c^2, where the background dominates the Λ signal.

The geometric acceptance of a $p\pi^-$ pair with an invariant mass in the Λ window is calculated using Monte Carlo simulation. Events are drawn for $\bar{p}d \to \Lambda K n \pi$ ($n=2,3$), assuming phase-space distribution. The decay products of the lambda are tracked through the detector, using the known efficiencies of the wire chambers. The

TABLE II. Observed and corrected multiplicity distribution (%) (both charge signs included). The statistical errors of the input quantities are less than 0.1%. For comparison, data from previous bubble-chamber experiments are given.

	^{1}H Seen	^{1}H Real	^{1}H Ref. 55[a]	^{1}H Ref. 56[a]	^{2}H Seen	^{2}H Real	^{2}H Ref. 23	^{12}C Ref. 7	^{14}N Seen	^{14}N Real
0	8.6	2.9 ±0.5	3.7 ±0.2	4.5 ±0.2	5.7	1.7 ±0.6	3.7 ±0.2	1.8 ±1.0	8.0	2.5 ±0.2
1	21.8				19.5	2.7 ±1.2	7.2 ±0.4	14.7 ±2.5	23.8	10.1 ±0.5
2	32.4	39.8 ±1.8	45.6 ±0.5	43.0 ±0.6	31.4	23.4 ±1.7	24.2 ±0.6	22.9 ±2.8	32.7	26.0 ±0.9
3	20.8				25.4	30.2 ±1.9	25.5 ±0.9	30.0 ±2.9	21.9	30.7 ±1.0
4	13.0	52.7 ±1.7	46.9 ±0.5	48.4 ±0.6	13.2	27.1 ±1.7	26.8 ±0.7	19.4 ±2.7	10.4	21.5 ±0.7
5	2.5				3.7	7.8 ±1.1	9.8 ±0.5	10.0 ±1.8	2.5	7.0 ±0.5
6	0.9	4.6 ±1.0	3.8 ±0.2	4.1 ±0.2	0.9	2.8 ±0.8	2.5 ±0.2	1.2 ±0.8	0.6	1.4 ±0.3
7					0.2	0.5 ±0.5	0.3 ±0.1		0.1	0.8 ±0.2
$\langle n_{\pi\pm} \rangle$		3.18 ±0.10	3.02 ±0.03	3.04 ±0.03		3.10 ±0.12	3.05 ±0.05	2.85 ±0.10		2.89 ±0.09

[a]Based on number of charged prongs given in the reference.

TABLE III. Net charge distributions (in %) observed in our and other experiments.

	^{2}H		^{14}N	^{12}C			
	Ref. 23[a]	Ref. 57[b]		Ref. 8	Ref. 9	Ref. 7	Ref. 10[c]
3			1.2	0.2	0.9	0.0	0.0
			±0.2	±0.1	±0.1		
2			3.9	2.1	1.8	5.3	2.2
			±0.4	±0.2	±0.2	±1.7	
1			14.2	17.5	12.5	15.2	12.0
			±0.8	±0.5	±0.4	±2.5	
0	55.0	57.2	57.1	39.5	38.3	43.0	39.2	42.8
	±2.6	±1.1	±3.0	±1.0	±0.8	±0.8	±2.9	
−1	45.0	42.8	42.9	31.1	33.7	34.5	37.4	34.7
	±2.6	±1.1	±3.0	±0.8	±0.7	±0.7	±2.9	
−2			8.0	7.8	6.5	2.9	8.0
			±0.5	±0.3	±0.3	±1.3	
−3			2.1	0.6	1.0	0.0	0.7
			±0.3	±0.1	±0.1		
$n(\pi^-)-n(\pi^+)$	45.0	42.8	42.9	27.8	34.5	33.0	17.4	35.9
All events	±2.6	±1.1	±3.0	±0.6	±2.1	±2.5	±5.7	
n_{π^+}/n_{π^-}	0.758	0.754	0.753	0.800	0.780	0.784		
	±0.008	±0.007	±0.012	±0.08	±0.012	±0.015		
$\langle n_{\pi^\pm}\rangle$	3.10	3.05	3.07	2.89	2.79	2.72	2.85	
	±0.12	±0.05	±0.08	±0.09	±0.04	±0.03	±0.10	
mean value		3.06		2.89		2.75		
		±0.04		±0.09		±0.02		
$\dfrac{\Delta\langle n_{\pi^\pm}\rangle}{\langle n_{\pi^\pm}\rangle}$				0.06		0.10		
				±0.03		±0.02		

[a]Derived from $\bar{p}n/\bar{p}p = 0.749\pm0.018$.
[b]Derived from $\bar{p}p/\bar{p}n = 1.33\pm0.07$.
[c]Intranuclear cascade model predictions.

main reasons for losing an event are too low pion energy and too low proton energy. Furthermore we correct for the unobserved neutral decay mode ($n\pi^0$) and for protons lost by the dE/dx cut. The loss is 29% for deuterium and 19% for nitrogen. In deuterium a higher cut needs to be set, because the pion to proton ratio is larger. Lastly we correct for those Λ's, which decay in the XDC or beyond (14%), where no dE/dx value can be determined. These quantities are listed in Table V. The background is calculated from a fit to the sidebins of the Λ with a third degree polynomial. Figure 8 shows the signal after background subtraction for deuterium and nitrogen. The ratio

$$B(\bar{p}\,{}^{14}\text{N}\rightarrow\Lambda+X)/B(\bar{p}\,{}^2\text{H}\rightarrow\Lambda+X)=2.1\pm0.4$$

is only slightly affected the different acceptance factors; without corrections one obtains a value of 2.4.

Because of insufficient vertex resolution, it is not possible to select a clean sample of lambda events. To construct a Λ-momentum spectrum we subtracted from the events in the signal region a background spectrum, using the sidebins in the invariant-mass spectrum. Within the albeit large statistical errors no striking difference between deuterium and nitrogen was found. The shape of the deuterium spectrum follows published bubble-chamber data.[37] The Λ spectrum may also be fitted with a Maxwell-Boltzmann ansatz. The temperatures

$$57\pm6 \text{ MeV } (\text{D}_2) \text{ and } 62\pm10 \text{ MeV } (\text{N}_2)$$

are similar to the proton case. The temperature and Λ yield for deuterium agree with previous data.[21,37]

The search for events in the exclusive channel $\bar{p}d\rightarrow\Lambda K_s\rightarrow(p\pi^-)(\pi^+\pi^-)$ yielded one single candidate, consistent with a background event from $\bar{p}d\rightarrow\Lambda K^+\pi^-$

TABLE IV. Multiplicity distribution of protons with momentum bigger than 170 MeV/c (^{2}H, ^{14}N) in %. Propane bubble-chamber data with visible protons are shown for comparison in the last column.

	^{2}H	^{14}N	^{12}C Ref. 9
0 protons	89.0±1.0	54.2±1.5	47.6±0.9
1 proton	10.6±0.9	27.3±1.0	29.3±0.7
2 protons	0.3±0.1	12.8±0.8	15.0±0.5
≥3 protons		5.7±0.6	8.2±0.4
$\langle n_p\rangle$		0.70±0.03	0.84±0.02
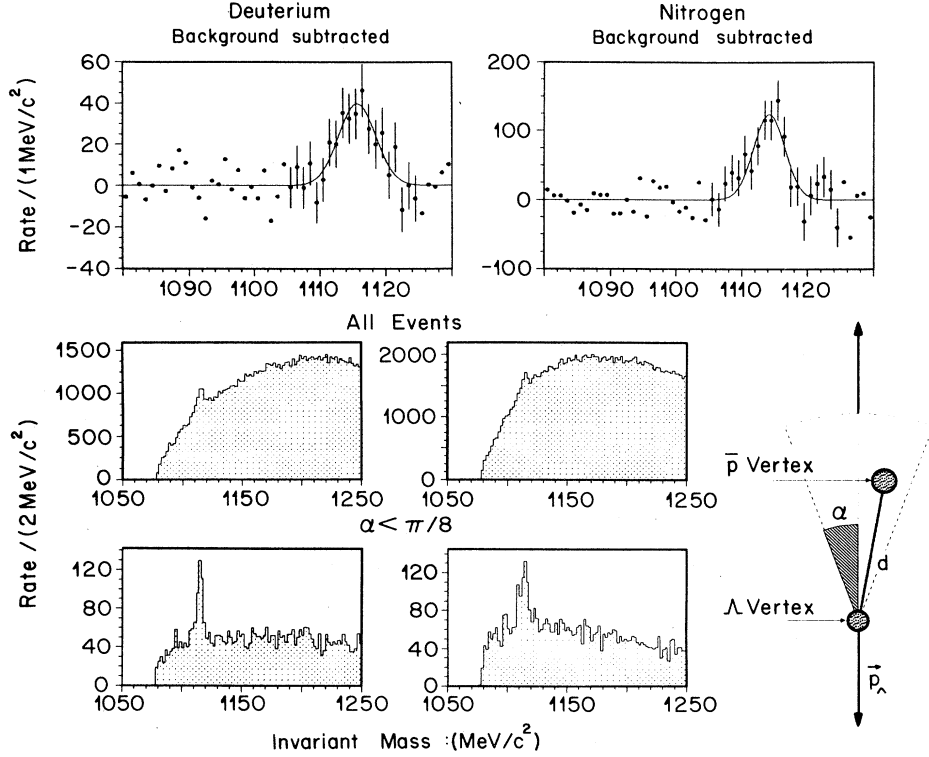
FIG. 8. The Λ signal in $\bar{p}d$ (left) and $\bar{p}N_2$ (right). Top and center: $\pi^- p$ invariant-mass spectra using the total statistics. Center: same as top, but with a cut around the Λ direction requiring the primary vertex to lie within a cone of opening angle α. Bottom: Used data samples for the calculation of the absolution cross sections after background subtraction (polynomial of third degree fitted to the sidebins).

with a K^+ misidentified as a π^+. This one event corresponds to an upper limit at a level of 10^{-5} for this channel.

The analysis of the channel $\bar{p}d \rightarrow \Lambda K^+ \pi^-$ uses the full data sample, corresponding to 2.1×10^6 stopping antiprotons. The event selection required four tracks (one proton candidate), zero total charge, and a $p\pi^-$ pair with an invariant mass in the Λ region. Under the assumption that the second positive charged track was a kaon, the energy balance $E_{bal} = E_\Lambda + E_{K^+} + E_{\pi^-} - 3m_p$ is calculated. The remaining 19 events with $|E_{bal}| \leq 120$ MeV and a missing momentum $|\mathbf{p}_{miss}| \leq 120$ MeV/c have been scanned optically. The Dalitz plot is shown in Fig. 9. In the K^+ spectrum we also included the seven events seen with a branching ratio of $(3.2 \pm 1.7) \times 10^{-5}$ in a bubble-

chamber experiment[30] and seven $\Lambda K^0 \pi^0$ events from the same experiment. We discuss the implications of these distributions for Λ production models below.

E. Collinear events in $\bar{p}$ ^{2}H annihilation

The selection of collinear $(\bar{p}d \rightarrow p\pi^-, p_\pi = 1247$ MeV/$c)$ and nearly collinear events $(\bar{p}d \rightarrow m^+ m^- n_s; m = \pi, K; p_\pi \simeq 930$ MeV/c, $p_K \simeq 800$ MeV/$c)$ is quite similar to the treatment to $\bar{p}p \rightarrow \pi^+ \pi^-, K^+ K^-$ data described in Ref. 5. In the plane containing the beam axis both outgoing tracks are collinear. The variable

$$t = \frac{p_l^1}{p_t^1} + \frac{p_l^2}{p_t^2}$$

is a measure of the collinearity of the tracks, where p_l^i denotes the momentum component parallel and p_t^i the component perpendicular to the beam axis.

In the perpendicular plane both tracks lie on a circle traversing the whole detector. The centers of curvature of both tracks should coincide. As a measure we used

$$\chi = \frac{\mathbf{x}_1 \times \mathbf{x}_2}{|\mathbf{x}_1| \times |\mathbf{x}_2|}$$

where $\mathbf{x}$ designates the vectors pointing to the centers of curvature.

TABLE V. Quantities leading to the absolute branching ratios for Λ production in deuterium and nitrogen.

Data	^{2}H	^{14}N
N (Signal)	281	738
Error from the fit	32	80
Acceptance	0.135±0.004	0.154±0.005
Number of $\bar{p}$	691 400	768 100
$B(\bar{p}d \rightarrow \Lambda + X)$ (10^{-3})	3.0±0.4	6.2±0.8
Bizarri et al.[30]	3.6±0.6	

$\bar{p}d \rightarrow \Lambda K \pi$
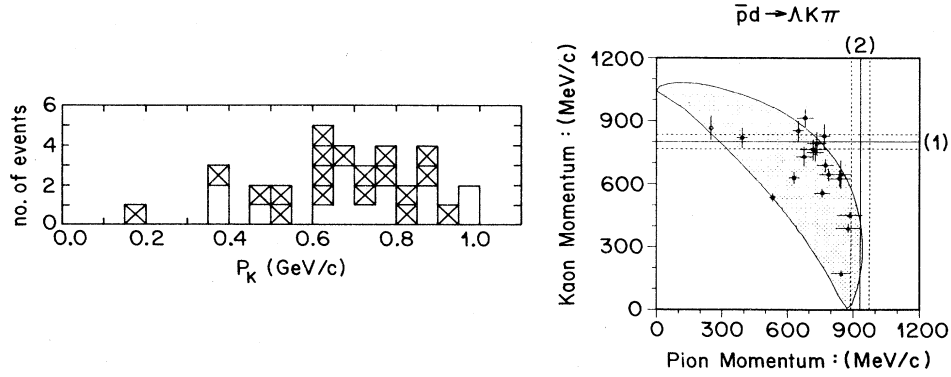
FIG. 9. Left: K momentum in $\bar{p}d \rightarrow \Lambda K^{+}\pi^{-}$. Open boxes: Ref. 30, hatched boxes: this experiment. Right: scatter plot pion versus kaon momentum, our data. The horizontal (vertical) band shows the regions of the two modes with the experimental momentum resolution indicated. $\bar{p}pn_s \rightarrow K^{+}(K^{-}n_s) \rightarrow K^{+}\pi^{-}\Lambda$ is expected with $p_K \approx 800$ MeV/c; $\bar{p}np_s \rightarrow \pi^{-}(\pi^{0}p_s) \rightarrow \pi^{-}K^{+}\Lambda$ with $p_\pi \approx 930$ MeV/c. The hatched areas show the region allowed from phase space $\bar{p}d \rightarrow \Lambda K^{+}\pi^{-}$.

After a preselection of all events with two tracks and different charges and both momenta larger than 500 MeV/c the variables t and χ are calculated. Figure 10 shows the region $[-0.2, 0.2]$ in t and $[0.996, 1.0]$ in χ for annihilation in hydrogen. The very sharp signal stems from $\pi^{+}\pi^{-}$ and $K^{+}K^{-}$. As these channels are not strictly collinear in deuterium due to Fermi motion, the same signal is broadened there (Fig. 10). The collinear events in deuterium for $\bar{p}d \rightarrow p\pi^{-}$ are suppressed by orders of magnitude and are not directly visible.

To understand the background we simulated the channels $\bar{p}p \rightarrow \pi^{+}\pi^{-}, K^{+}K^{-}, \bar{p}d \rightarrow p\pi^{-}$ and compared them to the data in hydrogen. The agreement is good. In deuterium the low-energy part of the spectator nucleon momentum spectrum can be approximated by a Gaussian distribution with center at 65 MeV/c and width of 32 MeV/c. The resulting Monte Carlo spectra for the channels $\bar{p}d \rightarrow \pi^{+}\pi^{-}(n_s)$ and $K^{+}K^{-}(n_s)$ reproduce the shape of the observed deuterium spectrum. The background comes from processes like $\bar{p}d \rightarrow \pi^{+}\pi^{-}\pi^{0}(n_s)$, where the spectrum is uniform in t while rising in χ. A fit with the sum of both contributions in the region $|t| \leq 0.2, \chi \geq 0.996$ fixes the background ratio of $3\pi n_s$ and the total ratio of $\bar{p}d \rightarrow \pi^{+}\pi^{-}(n_s)$ and $K^{+}K^{-}(n_s)$. The same region is used to determine the number of equivalent antiproton annihilations $N_{\text{total}} = 776\,800 \pm 51\,500$ used for the absolute branching ratios.

In the next step events with $|t| \leq 0.032, \chi \geq 0.999$ are selected and the appropriate fractions of $N[\pi^{+}\pi^{-}(n_s)]$, $N[K^{+}K^{-}(n_s)]$, and $N(3\pi n_s)$ surviving this cut are calculated by Monte Carlo simulation. For the selected events the average of both momenta is calculated and plotted in Fig. 10. The $\pi^{+}\pi^{-}n_s, K^{+}K^{-}\eta_s$ Monte Carlo simulations for this spectrum are fitted with Gaussian distributions which describe well the observed distribution within 3σ. The fit of the model curves contains a single free parameter, the relative fraction of $B(K^{+}K^{-}n_s)/B(\pi^{+}\pi^{-}n_s)$. The results are listed in Table VI. The acceptance for kaons is smaller due to decay. Since our event selection requires a low momentum spectator, but our results for the 3π and 5π channel described above show a channel-independent high-energy

spectator tail, a correction of 24% is applied. For a comparison to annihilations in pure hydrogen the rates are normalized to annihilation on the proton in deuterium (56%). The relative ratio

$$B(K^{+}K^{-}n_s)/B(\pi^{+}\pi^{-}n_s) = 0.36 \pm 0.08$$

is insensitive to the high-energy spectator tail or to the normalization to proton events and agrees with the value found for s-wave absorption in hydrogen.[5]
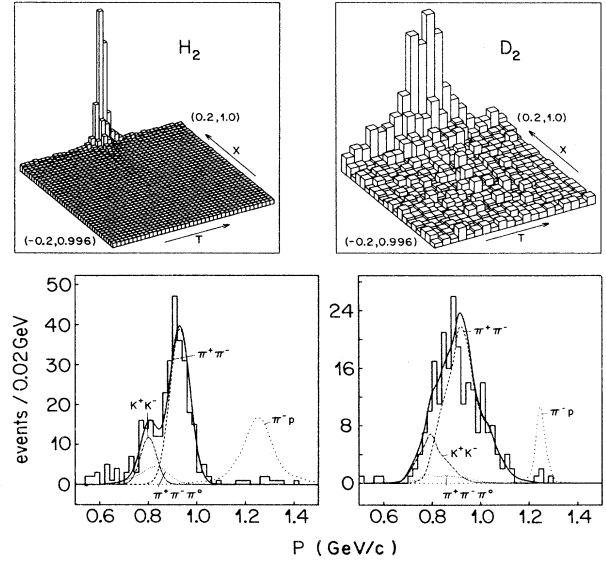
FIG. 10. Top: Collinearity spectra for hydrogen and deuterium (for an explanation of the variables see text). The sharp signal of the final states with two mesons in hydrogen in broadened in deuterium due to the spectator neutron. Bottom: Momentum spectra for $\bar{p}d \rightarrow \pi^{-}p, \pi^{+}\pi^{-}n_s, K^{+}K^{-}n_s$. Left: average of the measured momenta and fit on $\pi\pi/KK$ fraction ($\pi^{+}\pi^{-}\pi^{0}$ fixed from the selection criteria, shapes of the various contributions from Monte Carlo simulation), right: single helix fit to both tracks for selection of $\pi^{-}p$ events. The dotted lines with maximum at 1250 MeV/c represents the shape of the expected $p\pi^{-}$ signal, calculated with Monte Carlo simulation.

TABLE VI. Branching ratios for two mesons in the final state in deuterium ($\bar{p}d \rightarrow \pi^- \pi^+ n_s$, $\bar{p}d \rightarrow K^+ K^- n_s$) and for comparison in hydrogen.

Branching ratios $\pi\pi/KK$	$\pi^- \pi^+$	$K^+ K^-$
Events: $\chi \geq 0.999, \|t\| \leq 0.032$	$223 \pm 9_{Sys} \pm 15_{Stat}$	$55 \pm 9_{Sys} \pm 7_{Stat}$
Acceptance	0.1917	0.1305
Events with low-energy neutron	1163	421
Total number of events	1564	566
$B(\bar{p}d \rightarrow M^+ M^- n_s) \times 10^{-3}$	2.01 ± 0.27	0.73 ± 0.16
$B(\bar{p}d \rightarrow M^+ M^- n_s)/B(\bar{p}d \rightarrow Xn_s) \times 10^{-3}$	3.59 ± 0.40	1.30 ± 0.28
Ref. 58	4.2 ± 1.2	
$B(\bar{p}p \rightarrow M^+ M^-)$: s wave, Ref. 5	3.33 ± 0.17	1.01 ± 0.05
$B(\bar{p}p \rightarrow M^+ M^-)$: p wave, Ref. 5	4.81 ± 0.49	0.287 ± 0.051

Eleven events are observed in the momentum region [1150,1500] MeV/c. The Monte Carlo simulation for the three background channels gives 5.5 events for this region. With the known total number of antiprotons and an acceptance of 0.51 we obtain an absolute branching ratio of

$$B(\bar{p}d \rightarrow \pi^- p) = (1.4 \pm 0.7) \times 10^{-5} .$$

To get a good separation of the channels $\bar{p}p \rightarrow \pi^+ \pi^-, K^+ K^-$ from the background in hydrogen, all measured hits are combined into a single helix fit. The same algorithm is applied now for deuterium to reduce the background in the region of the $p\pi^-$ signal. With the additional requirements that both tracks reach at least the MWPC P_1 and have a measured momentum larger than 1150 MeV/c, none of the 100 000 generated events appear in the narrower signal region [1200,1300] MeV/c. Three events remain in the data. With an acceptance of 0.3 this leads to an absolute branching ratio of $(1.3 \pm 0.8) \times 10^{-5}$ in agreement with the previous number. The simulated background corresponds to a branching ratio of 2×10^{-8} and therefore the probability to find three events within 776 800 annihilations is less than 10^{-6}. In nitrogen the collinearity criteria cannot be used to look for the $\pi^- p$ channel, because the residual nucleus carriers momentum too. A possible signal for this process can therefore not be distinguished from the background.

F. Multimeson absorption

The term "multimeson absorption" refers to the interaction of a resonance, such as η, ω, or ρ with the remaining nucleons in the nucleus. Iljinov et al.[16] suggested to investigate η (and ω) absorption on a correlated nucleon pair via the process $\eta(pp) \rightarrow pp$, a reaction not unlike the well-known pion absorption $\pi^+ d \rightarrow pp$. As long as the η momentum is not too large, the proton pair will be emitted at large opening angles ($\theta_{pp} > 150°$) and with high energies ($T_p > 150$ MeV). Of all nitrogen events 8.5% had two detected protons and 3.0% three protons, leading to a data sample of 10^5 proton pairs. We tried to identify the mass of the absorbed resonance x via the relation

$$x(pp) \rightarrow p_1 p_2$$

$$m_x^2 = E_x^2 - p_x^2 = (E_1 + E_2 - m_{pp})^2 - (\mathbf{p}_1 + \mathbf{p}_2)^2$$

$$\cong (T_1 + T_2 + Q)^2 - (\mathbf{p}_1 + \mathbf{p}_2)^2 .$$

Such a procedure would be correct for a free diproton target at rest, or for the reaction $\pi^+ d \rightarrow pp$, i.e., the ab-
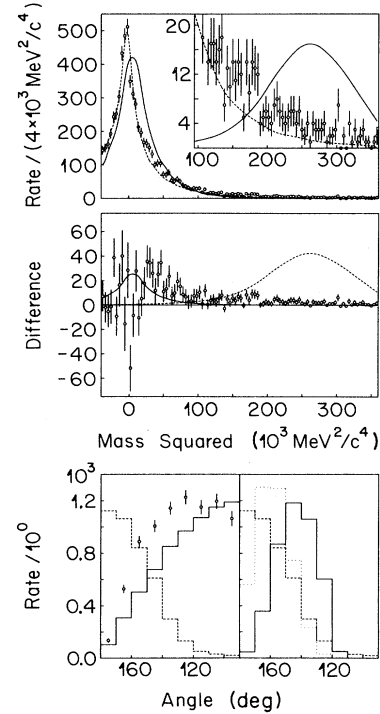
FIG. 11. Top and center: Reconstructed squared mass of meson absorbed on two nucleons in ^{14}N giving two protons in the final state. The dashed line (top) shows the background fraction based on two single protons with empirical momentum and random opening angle. Center: Background subtracted spectrum with pion absorption (solid line) according to the remaining fraction and η absorption (dashed line) with arbitrary scale. Bottom: Opening angle of two protons. Left: Data with background (solid histogram) scaled on (90°,120°) and prediction of η absorption in carbon.[16] Right: Comparison of simple Monte Carlo calculations for π absorption (solid line), η absorption (dotted line), and the prediction of Ref. 16 (dashed line).

sorption on an (np) pair. For the peak of the π (η) momentum distribution in $\bar{p}p$ annihilation $p_\pi \sim 300$ MeV/c $(p_\eta \sim 500$ MeV/$c)$ the proton angular distribution would peak at the minimum opening angle of $150°$ $(149°)$ with $p_1 = p_2 = 580$ MeV/c $(912$ MeV/$c)$. However, in our case the diproton is bound in a mass-13 system, and is moving with a momentum of the order of the Fermi momentum. Since the exact state of a unobserved eleven remaining nucleons is not known, one can only approximately correct for the binding energy $(Q \cong 22$ MeV), but not for the missing momentum and fortunately small kinetic energy. The absorption signal in the two-proton–invariant-mass distribution will therefore be broad. Figure 11 shows this distribution after a cut eliminating events with $\cos\theta_{pp} > -0.9$. The peak near $m_x^2 = 0$ arises as a consequence of the angle cut. The observed distribution can be reproduced by pairing at random two protons, each with its measured momentum distribution. Hence we do not find evidence for resonance assumption. To estimate upper limits, we have tried to obtain a simple guess of the expected signal shape in the m_x^2 distribution with the following method. Events were generated according to phase space for the reaction $x + m_{13} \rightarrow m_{11} + p + p$, with $m_{13} = \frac{1}{2}[m(^{13}\text{N}) + m(^{13}\text{C})]$ and $m_{11} = \frac{1}{2}[m(^{11}\text{B}) + m(^{11}\text{Be})]$ and a x momentum distribution given by Maxwell-Boltzmann distribution as measured here for pions and in Refs. 43 and 44 for η, if one ignores the influence of the $\eta\rho$ channel (14% of all).

For the reconstruction of the mass spectrum only events were retained for which the unobserved m_{11} momentum did not exceed the Fermi-momentum limit of 270 MeV/c and where the protons were within the geometrical limits of our detector and above the momentum threshold. The resulting curves are given in Fig. 11. As expected, they are quite broad, namely $\Delta(m_\pi^2)/m_\pi^2(\text{FWHM}) \cong 2.3$ and $\Delta(m_\eta^2)/m_\eta^2(\text{FWHM}) \cong 0.5$. The calculated width for the pion curve, however, is quite similar to that measured in pion absorption experiments [e.g., ^3He $\pi^+ \rightarrow ppp$, $\Delta(m_\pi^2)/m_\pi^2(\text{FWHM}) \cong 2.7$, $p_\pi = 270$ MeV/c, Ref. 45]. If we ascribe all events seen within a 42% confidence interval around the expected peak position to the $\pi(\eta,\omega)$ absorption process we obtain the following upper limits $B(x)$ for resonance absorption on two protons:

$$B(\pi) < 6\%, B(\eta) < 0.09\%, B(\omega) < 0.008\% \ .$$

More realistic limits are obtained if the random distribution (adjusted at $m_x^2 < 0$) is subtracted first, namely

$$B(\pi) < 0.3\% \text{ and } B(\eta) < 0.05\% \ .$$

This is shown in Fig. 11 together with the two-proton angular distribution for $T_p > 150$ MeV to facilitate comparison with the curves computed by Iljinov *et al.*[16]

III. DISCUSSION OF RESULTS

A. Comparison with intranuclear cascade model calculations

Unfortunately, calculations have not been performed for $A = 14$ and antiproton absorption at rest. However,

the results available for various nuclei, e.g., for the pion and η absorption probability at $p_{\bar{p}} = 608$ MeV/c,[46] indicate that the dependence on target mass is weak, e.g., proportional to $A^{1/3}$ in this case. Since calculations and some supplementary data exist for $A = 12$ and 20 we may suitably interpolate to compare with our data. Similarly, the dependence of relative branching ratios on the $\bar{p}$ momentum is smooth,[46] thus extrapolation to $\bar{p}$ at rest is acceptable, too. For the high-energy tail of the pion and proton inclusive spectra the intranuclear cascade (INC)[19] would thus predict for ^{14}N at rest the temperatures $T_0(p) = 69$ MeV (Ne value) and $111 < T_0(\pi) < 140$ MeV, while we measure 66 MeV and 131 MeV, respectively. In view of the uncertainties of the INC calculation and the failure of microscopic calculations to predict the high-energy proton tail in the deuterium case (see below), we do not rate this agreement very high. Furthermore, we have used a Lorentz-invariant form of the Maxwell-Boltzmann distribution, while the theoretical results apply for the nonrelativistic form (without the factor E^{-1}, see Sec. II B). Our data, however, do not show the change in slope near $p_\pi = 200$ MeV/c, appearing in the predictions, and the data for $p_{\bar{p}} = 608$ MeV/c on ^{12}C (Ref. 15) and ^{20}Ne (Ref. 14). Such a reduction has been interpreted as evidence for πN interaction in the Δ region.[19,24,25] In our $(\pi^- p)$ invariant-mass spectrum constructed for the Λ signal no strong Δ^0 signal appears either. In the absence of a model for the uncorrelated background in the $\pi^- p$ mass spectrum, no quantitative upper limit for such a signal can be given.

A quantity, which has been used to compare the treatment of pion and resonance absorption in the models, with the data,[19] is the decrease of the mean pion multiplicity for different targets. This approach is, however, not sensitive for the following reasons: The measured multiplicities come from different experiments, e.g., the ^{12}C data from propane bubble chamber,[7,9] where the ratio of $\bar{p}$ absorption in ^1H and ^{12}C needs to be known, or from solid targets placed in liquid hydrogen,[8] where target shadowing effects lead to large corrections and the antiprotons are not necessarily at rest. Comparison for a $Z = N$ nucleus must be made to deuterium bubble-chamber results.[23] We avoided this problem by comparing directly ^{14}N and d in the same detector, but the incomplete solid angle increased our uncertainty, too. Consequently the comparison made in Table III shows that the reduction of multiplicity for the light systems $(A = 12, 14)$ is only measured with large error bars. Furthermore the loss of π^+ and π^- due to absorption is partly offset by charge exchange (CE), where more π^+ and π^- are expected to be produced by π^0 than converted into π^0. In the very naive ansatz, where an average $\pi^0 \leftrightarrow \pi^-, \pi^+$ conversion probability (f_{CE}) is multiplied with the remaining number of nucleons, and the ratio of $\bar{p}n$ to $\bar{p}p$ absorption is taken from deuterium $(r = \bar{p}n/\bar{p}p \cong \frac{3}{4})$ with $\bar{p}n \rightarrow \pi^+ 2\pi^- 2\pi^0$ and $\bar{p}p \rightarrow 1.5\pi^+ 1.5\pi^- 2\pi^0$ (on average), one expects the number of π^- $[\pi^+]$ to increase by $\cong \frac{5}{7} f_{\text{CE}}(Z-1)$ $[\cong \frac{2}{7} Z f_{\text{CE}}]$ for $Z = N$ systems. That the average exchange probability is fairly large is apparent from the net multiplicity distributions (Table II), which show rather large entries for

$Q = \pm 2e$. Iljinov et al.[16] have computed this distribution for ^{12}C and found fair agreement; however, their calculation started from $r=1$, which is different from deuterium and not justified for ^{12}C and ^{14}N either in view of the fact that the measured π^+/π^- ratio varies little from ^{2}H to ^{14}N. In fact this ratio, which is the best measured quantity, may be used to estimate f_{CE}. In our naive model, this ratio varies as

$$\frac{\pi^+}{\pi^-}(Z) \cong \frac{\pi^+}{\pi^-}(^2H)\left[1 + \frac{7}{18}f_{CE}(Z-1)\right].$$

The increase with Z is indeed observed and consistent with $f_{CE} \cong (1.8\pm0.6)\%$. This naive model also explains why the difference between the number of observed π^- and π^+ decreases with Z and can therefore not be taken as evidence for a decrease of r in nuclei, as done in Refs. 8 and 9, and further as evidence for a neutron halo around the nucleus, an interpretation which Iljinov et al.[16] questioned, too. Within this reasoning a 10% increase of $\langle n_{\pi\pm}\rangle$ due to charge exchange is then expected while the overall decrease of $\langle n_{\pi\pm}\rangle$ is only 6±3%. For 600 MeV/c the available predictions vary between 4.7 and 17% for this reduction. Future cascade calculations should have no problems addressing these points in greater detail by looking both at multiplicity as well as net charge. Furthermore the use of direct absorption signals, like we have tried with the (pp) correlations, seems a more promising route, at least for pions, once more statistics and better predictions are available.

For η absorption our data do not support the optimism of the early calculations,[10] which lead us to expect a strong signal. In fact these predictions (e.g., angular distributions shown in Fig. 11) do not agree with our data and our simple Monte Carlo model. However, we are quite in agreement with the statement[46] that, "a possible signal will be lost in the background of the pairs of protons produced in the cascade process."

Since 0.07 η are created per annihilation ($\bar{p}p$),[43] the prediction[46] that 28% of these will be absorbed would be more directly and easily measurable with a dedicated η detector, such as the proposed Crystal Barrel.[47] Disappearance of η and ω has also been suggested[46] to contribute to the Λ yield, via $\omega N \rightarrow \Lambda K, \eta N \rightarrow \Lambda K$. At 608 MeV/$c$ the predicted yield $\bar{p}A \rightarrow \Lambda X$ via these processes account for roughly $\frac{1}{3}$ of the observed yield of 1.95±0.43% (Ref. 14) in ^{20}Ne (in ^{12}C for $p_{\bar{p}} \le 459$ MeV/c, 2.3±0.6% is measured[11]). At $p_{\bar{p}}=0$ a yield of 0.5% is calculated for Ne. Scaled by $A^{1/3}$ this would correspond to 70% of the yield measured by us. This large estimate precludes at present the interpretation of the Λ yield as a signal for two nucleon absorption. For $B=1$ ($\bar{p}NN$) the strange particle yield increases compared to $B=0$. Including Σ decays 4.7% Λ per annihilation could be produced in this absorption model.[28] Our data would therefore limit the $B=1$ contribution to less than 13% of the $B=0$ contribution. We will return to this problem in the following section.

B. Two-nucleon absorption channels in deuterium

The relative yield for events with high-energy protons from ^{14}N and ^{2}H

$$B(\bar{p}\,^{14}N \rightarrow p + x)/B(\bar{p}\,^2H \rightarrow p + x) = 4.2\pm0.4$$

is compatible with the ratio of nucleons on the surface. The restriction to exclusive channels in antiproton deuteron annihilation, like $\bar{p}d \rightarrow 3\pi p_s$ or $5\pi p_s$ allows a closer view, because realistic nucleon potentials and pion scattering amplitudes can be used. Here the inclusion of the Δ resonance, first studied by Alberi et al. at intermediate energies,[48] is a debated issue and could change the fraction of rescattering processes. Apart from simple models using incoherent two-step processes, there exists one detailed calculation[37] for $\bar{p}d \rightarrow 5\pi p_s$, where all possible triangle diagrams are included. Because this work still ignores spin effects and other small corrections, the results are not considered final, but they underestimate the experimental spectrum by a factor of 4, a fact which has been seen in the channel $\bar{p}d \rightarrow K\bar{K}2\pi p_s$ too.[36] Zemany et al.[49] found 28.1±1.7% (31.6±1.6%) of all $5\pi p_s$ ($3\pi p_s$) events with a high momentum spectator proton. However since they measured at an initial antiproton momentum of 1.3 GeV/c, they ascribe 6.4±0.7% (5.3±0.4%) to initial-state interaction, which should be strongly suppressed at rest.

From these considerations it is clear that to find evidence for possible nonstandard annihilation mechanisms one should look at exclusive channels, where predictions include realistic properties of the deuteron. A promising channel in this respect is $p\pi^-$, which allows to compare different approaches. The first six events seen in a bubble chamber[30] at a branching ratio of $(0.9\pm0.4)\times10^{-5}$ were interpreted as originating from a three-body interaction. This statement requires an overlap of the proton and the neutron wave function. This can be visualized as a continuous shrinking of the triangle in Fig. 1 to a single vertex with total baryon number $B=1$. In more fashionable language this overlap arises from the quark compound-bag model,[50] where the deuteron exists at a level with 10% probability as a six quark state. On the quark level a rearrangement and an annihilation graph of the quark lines, analogous to $\bar{p}p \rightarrow \pi^+\pi^-$, can be drawn. Alternatively this reaction may be viewed as a two-step process where in the first step the antiproton annihilates on a single nucleon giving two mesons and in the second step one meson is absorbed on the remaining spectator nucleon. The calculations[51] depend strongly on the off-shell meson form factors and the deuteron wave functions. Realistic models (Paris or Reid Potentials) lead to branching ratios less than 10^{-6}, and so this mechanism cannot describe the measured values $(1.4\pm0.7)\times10^{-5}$, $(0.9\pm0.4)\times10^{-5}$ (Ref. 30), and $(2.8\pm0.3)\times10^{-5}$ (Ref. 13). On the other hand Oset and Hernandez argue[52] that the absorption on the free spectator nucleon can only proceed via virtual mesons, which they call meson exchange current mechanism (in contrast to final-state interaction with on-shell mesons). As the phase between $\bar{p}pn \rightarrow \pi^-\pi^+n \rightarrow \pi^-p$ (π^+ intermediate) and $\bar{p}np \rightarrow \pi^-\pi^0p \rightarrow \pi^-p$ (π^0 intermediate) is not known, they find a branching ratio within the interval $[0.6\times10^{-5}, 14.7\times10^{-5}]$ in the correct order of magnitude.

The high rate of Λ production in $\bar{p}d$ at rest has been interpreted as evidence for a three-body interaction,[30] because scattering of primary kaons on the remaining spec-

tator creating $\Lambda\pi$ could not explain the yield. In nitrogen, neither the angular momentum nor momentum of the spectators is necessarily low, making a prediction more difficult. In this context, however, the similarity of the Λ-momentum spectra for ^{2}H and ^{14}N is worth noting. The channel $\bar{p}d \rightarrow \Lambda K\pi$ is particularly well suited to study incoherent rescattering in unique kinematical situations. The possible two-step production mechanisms for a Λ can be written as

$$(\bar{p}p)n \rightarrow K^+(K^-n) \rightarrow K^+\pi^-\Lambda \tag{1}$$

$$(\bar{p}p)n \rightarrow \pi^-(\pi^+n) \rightarrow \pi^-K^+\Lambda \tag{2a}$$

$$(\bar{p}n)p \rightarrow \pi^-(\pi^0p) \rightarrow \pi^-K^+\Lambda \tag{2b}$$

with $|\mathbf{p}_K| = 797$ MeV/c in the first case and $|\mathbf{p}_\pi| = 928$ MeV/c in the second cases. This type of analysis was pioneered by Bizarri *et al.*,[30] who neglected processes (2a) and (2b) because of the low cross sections for $\pi n \rightarrow K\Lambda$ at $p_\pi = 928$ MeV/c. Figure 9 shows the kaon momentum of the 12 entries from the latter experiment and our 19 candidates. No strong enhancement at 800 MeV/c is visible. But since the production rate for $\pi\pi$ exceeds that for $K\bar{K}$ by a factor of 3 and n as well as p can contribute, pion rescattering should be taken into account. A quantitative calculation[37] of both modes and a comparison to the Λ-momentum spectrum could not fit the data but gave only a small fraction for the pion rescattering mode. Figure 9 shows a two-dimensional plot of both momenta. From nineteen entries nine can be assigned to process (1) and three to reaction (2). The remaining seven events could then be regarded as evidence for a direct production mechanism of the Λ. It is clear that dedicated deuterium experiments at LEAR should be promoted to answer these questions seriously. Then it would be possible to find out whether virtual exchange particles do increase production rates as in the $p\pi^-$ channel. Also, the influence of resonances like η, ω, or even ρ on the spectator,[53] with less restricted phase space for Λ production could be tested. For future calculations it may be helpful to bear in mind that our results for the $\pi^+\pi^-\eta_s/K^+K^-n_s$ branching indicate that the $\bar{p}p$ initial state in deuterium is dominantly s wave for gas (STP).

In our opinion the most successful way to look for unusual annihilation mechanisms in the future lies in the spectroscopy of exclusive channels where precise theoretical predictions can be made. General features like baryon production or particle multiplicities are consistent with simple rescattering processes in first order and no striking effect can be found. The same holds for multimeson interactions.

ACKNOWLEDGMENTS

[a]Present address: KEK, Tsukuba, Ibaraki 305, Japan.

[b]Present address: University of Toronto, Ontario, Canada M5S 1A7.

[c]Present address: Max Planck Institut, 8000 München, Germany.

[d]Present address: Schott Glaswerke, 6500 Mainz, Germany.

[e]Present address: Boehringer, 6507 Ingelheim, Germany.

[f]Present address: Volkshochschule, 6450 Hanau, Germany.

[g]Present address: AT&T, 8000 München, Germany.

[h]Present address: GEI, 6100 Darmstadt, Germany.

[i]Present address: LeCroy Research Systems, 1211 Genève, Switzerland.

[j]Present address: AMESA Technologies, 1219 Genève, Switzerland.

[k]Present address: DVFLR, 7000 Stuttgart, Germany.

[l]Present address: TRIUMF, Vancouver, B.C., Canada V6T 2A3.

[m]Present address: Salomon, Annecy, France.

[n]Present address: Österreichische Akademie der Wissenschaften, 1050 Wien, Austria.

[o]Present address: Voest Alpine, 1011 Wien, Austria.

[1]S. Ahmad *et al.* (submitted to Nucl. Instrum. Methods).

[2]*Physics at LEAR with Low Energy Antiprotons,* edited by C. Amsler *et al.* Nucl. Sci. Res. Conf. Ser. 14 (Harwood Academic, Chur, Schweiz, 1988).

[3]R. Landua, Proceedings of the Ninth European Symposium on Proton-Antiproton Interactions and Fundamental Symmetries, Mainz, 1988, edited by K. Kleinknecht and E. Kempt [Nucl. Phys. B (Proc. Suppl.) **8**, 179 (1989)]; S. Ahmad *et al.*, Ref. 2, p. 405.

[4]S. Ahmad *et al.*, Phys. Lett. **157B**, 333 (1985); M. Zeigler *et al.*, *ibid.* **206**, 151 (1988); G. Reifenröther *et al.*, *ibid.* **214**, 325 (1988); U. Schaefer *et al.*, Nucl. Phys. **A495**, 451 (1989).

[5]S. Ahmad *et al.*, Phys. Lett. **152B**, 136 (1985); M. Doser *et al.*, *ibid.* **215**, 792 (1988); M. Doser *et al.*, Nucl. Phys. **A486**, 493 (1988).

[6]S. Ahmad *et al.*, *Proceedings of the International Conference on Antinucleon- and Nucleon-Nucleus Interactions, Telluride, Colorado, 1985,* edited by G. E. Walker *et al.* (Plenum, New York, 1985), p. 73.

[7]L. Agnew *et al.*, Phys. Rev. **118**, 1371 (1960).

[8]W. M. Bugg *et al.*, Phys. Rev. Lett. **31**, 475 (1973).

[9]M. Wade and V. G. Lind, Phys. Rev. D **14**, 1182 (1976).

[10]G. T. Condo, T. Handler, and H. O. Cohn, Phys. Rev. C **29**, 1531 (1984).

[11]G. T. Condo, W. M. Bugg, T. Handler, and H. O. Cohn, Phys.

Lett. **144B**, 27 (1984).

[12]A. G. Ekspong, Å. Frisk, S. Nilsson, and B. E. Ronne, Nucl. Phys. **22**, 353 (1961).

[13]G. A. Smith, in *The Elementary Structure of Matter*, Vol. 26 of *Springer Proceedings in Physics*, edited by J. M. Richard *et al.* (Springer, Heidelberg, 1988), p. 219; and Pennsylvania State University Report PSU HEP/87-14 (1987); T. Armstrong *et al.*, Z. Phys. A **332**, 467 (1989); A. Angelopoulos *et al.*, Phys. Lett. B **205**, 590 (1988).

[14]F. Balestra *et al.*, Phys. Lett. B **194**, 192 (1987); **217**, 43 (1989); Nucl. Phys. **A452**, 576 (1986).

[15]P. L. McGaughey, Phys. Rev. Lett. **56**, 2156 (1986).

[16]A. S. Iljinov, V. I. Nazaruk, and S. E. Chigrinov, Nucl. Phys. **A382**, 378 (1982).

[17]Ye. S. Golubeva, A. S. Iljinov, A. S. Botvina, and N. M. Sobolevsky, Nucl. Phys. **A483**, 539 (1988).

[18]For a review see J. Cugnon and J. Vandermeulen, Ann. Phys. (Paris) **14**, 49 (1989).

[19]J. Cugnon, P. Deneye, and J. Vandermeulen, Nucl. Phys. **A500**, 701 (1989).

[20]M. R. Clover, R. M. DeVries, N. J. DiGiacomo, and Y. Yariv, Phys. Rev. C **26**, 2138 (1982); P. L. McGaughey, M. R. Clover, and N. J. DiGiacomo, Phys. Lett. **166B**, 264 (1986).

[21]J. Roy, in *Proceedings of the Fourth International Symposium on Nucleon-Antinucleon Interactions, Syracuse, 1975*, edited by T. Kalogeropoulos and K. C. Wali (Syracuse University Press, Syracuse, NY, 1975), p. III-1.

[22]T. Kalogeropoulos, L. Gray, A. Nandy, and J. Roy, Phys. Rev. D **24**, 1759 (1981).

[23]T. Kalogeropoulos and G. S. Tzanakos, Phys. Rev. D **22**, 2585 (1980).

[24]E. Hernández and E. Oset, Nucl. Phys. **A455**, 584 (1986).

[25]J. H. Kim and H. Toki, Prog. Theor. Phys. (Lett.) **72**, 1050 (1984).

[26]R. Armenteros *et al.*, Ref. 2, p. 507.

[27]B. H. Pontecorvo, Zh. Eksp. Teor. Fiz. **3**, 1143 (1956) [Sov. Phys.—JETP **30**, 947 (1956)].

[28]J. Cugnon and J. Vandermeulen, Phys. Rev. C **39**, 181 (1989).

[29]E. Hernández and E. Oset, Phys. Lett. B **184**, 1 (1987).

[30]R. Bizzari *et al.*, Lett. Nuovo Cimento **2**, 431 (1969).

[31]D. Strottmann, Phys. Lett. **119B**, 39 (1982).

[32]See review given by J. Rafelski, Addendum to Ref. 2; Phys. Lett. B **207**, 371 (1988).

[33]C. Dereth, W. Greiner, H. T. Elze, and J. Rafelski, Phys. Rev. C **31**, 1360 (1985).

[34]S. C. Phatak and N. Sarma, Phys. Rev. C **31**, 2113 (1985).

[35]K. Miyano *et al.*, Phys. Rev. Lett. **53**, 1725 (1984); Phys. Rev. C **38**, 2788 (1988).

[36]B. Y. Oh *et al.*, Nucl. Phys. **B51**, 57 (1973).

[37]M. Locher, International Conference on Medium- and High-Energy-Physics, Taipei, Republic of China, 1988 (unpublished); S. Nozawa and M. Locher, Ref. 2, p. 763.

[38]E. Hernández and E. Oset, Nucl. Phys. **A493**, 453 (1989).

[39]S. Ahmad *et al.*, Ref. 2, p. 697; J. Riedlberger *et al.* (unpublished).

[40]H. Poth *et al.*, Nucl. Phys. **A294**, 435 (1978).

[41]D. Bridges *et al.*, Phys. Rev. Lett. **56**, 211 (1986); **56**, 215 (1986); **57**, 1534 (1986).

[42]S. Ahmad *et al.*, Ref. 2, p. 447.

[43]M. Chiba *et al.*, Ref. 2, p. 401.

[44]L. Tauscher *et al.*, Ref. 2, p. 397.

[45]G. Backenstoss *et al.*, Paul Scherrer Institut—Villigen (CH) Report 88-24 (1988).

[46]J. Cugnon, P. Deneye, and J. Vandermeulen (unpublished).

[47]E. Aker *et al.*, Ref. 2, pp. 493 and 503.

[48]G. Alberi *et al.*, Nuovo Cimento **53A**, 191 (1979); Nucl. Phys. **108B**, 327 (1976).

[49]P. D. Zemany, Z. Ming Ma, and J. M. Mountz, Phys. Rev. Lett. **38**, 1443 (1977).

[50]A. I. Veselov, Yu. S. Kalashnikova, and I. M. Narodetskii, Yad. Fiz. **42**, 550 (1985) [Sov. J. Nucl. Phys. **42**, 347 (1985)]; A. I. Veselov, I. L. Grach, Yu. S. Kalashnikova, and I. M. Narodetskii, Yad. Fiz. **44**, 21 (1986) [Sov. J. Nucl. Phys. **44**, 14 (1986)]; Yu. S. Kalashnikova and I. M. Narodetskii, Yad. Fiz. **42**, 324 (1985) [Sov. J. Nucl. Phys. **42**, 203 (1985)]; Yu. S. Kalashnikova, I. M. Narodetskii, Yu. A. Simonov, and A. I. Veselov, Phys. Lett. **155B**, 217 (1985).

[51]L. A. Kondryatuk and M. G. Sapozhnikov, Ref. 2, p. 771; Phys. Lett. B **220**, 333 (1989).

[52]E. Oset and E. Hernández, Ref. 2, p. 753.

[53]D. E. Kharzeev and M. G. Sapozhnikov, Joint Institute of Nuclear Research—Dubna Report E4-88-930 (submitted to Phys. Lett. B).

[54]T. E. Kalogeropoulos, Proceedings of the Seminar on Interactions of High-Energy Particles with Nuclei and New Nuclear-Like Systems, Moscow, 1973 (unpublished).

[55]C. Baltay *et al.*, Phys. Rev. **145**, 1103 (1966).

[56]J. Díaz *et al.*, Nucl. Phys. **16B**, 239 (1970).

[57]W. Chinowsky and G. Kojoian, Nuovo Cimento **43A**, 684 (1966).

[58]L. Gray *et al.*, Phys. Rev. Lett. **30**, 1091 (1973).